Engineering Failure Analysis 60 (2016) 20–39

Contents lists available at ScienceDirect

Engineering Failure Analysis

journal homepage: www.elsevier.com/locate/engfailanal

A repertoire of failures in connecting rods for internal combustion engines, and indications on traditional and advanced design methods

A. Strozzi, A. Baldini, M. Giacopini *, E. Bertocchi, S. Mantovani

Department of Engineering "Enzo Ferrari", University of Modena and Reggio Emilia, Modena, Italy

ARTICLE INFO

Article history:
Received 27 May 2015
Received in revised form 10 November 2015
Accepted 16 November 2015
Available online 18 November 2015

Keywords:
Connecting rod
Shank
Small end
Big end
Failure
Buckling
Fatigue
Fretting fatigue
Cavitation

ABSTRACT

Several typical and uncommon failure modes in con-rods for internal combustion engines are commented from the stress level viewpoint. The interpretation of the fractures is supported with traditional calculations, with more advanced analytical models, and with Finite Element (FE) predictions. The repertoire of failures in a con-rod is presented by separately addressing the parts composing the con-rod itself, namely the shank, and the small and big ends.

1. Introduction

The connecting rod is one of the most important components employed in internal combustion engines. Its extremities are shaped as eyes, named con-rod small end (upper) and con-rod big end (lower), connected by a beam-like shank. The small end of the connecting rod is joined to the piston by means of the gudgeon pin, whereas the big end is mounted on the crank-pin of the crankshaft. The function of the connecting rod is to translate the alternating transverse motion of the piston to the rotational motion of the crankshaft.

Making part of the engine, the connecting rod is subjected to high-cycle fatigue loading. Contributions due to both gas forces and inertial forces have to be considered. The connecting rod has to be strong enough to bear the external loading, rigid enough to allow a correct coupling with the gudgeon pin and the crank-pin and, at the same time, it has to be light enough to minimize the inertial forces derived from its motion. In particular, a certain portion of the connecting rod may be considered as an alternating mass, thus directly affecting the maximum value of the alternating forces. As a consequence, particular care has to be devoted to the connecting rod design process. Both analytical and numerical methods are usually employed for connecting rod optimization [1–4].

The collapse of a connecting rod is among the commonest causes of catastrophic engine failure. This paper presents several typical and uncommon failure modes of connecting rods employed in internal combustion engines, and it reports an explanation

* Corresponding author.
E-mail address: matteo.giacopini@unimore.it (M. Giacopini).

http://dx.doi.org/10.1016/j.engfailanal.2015.11.034
1350-6307/

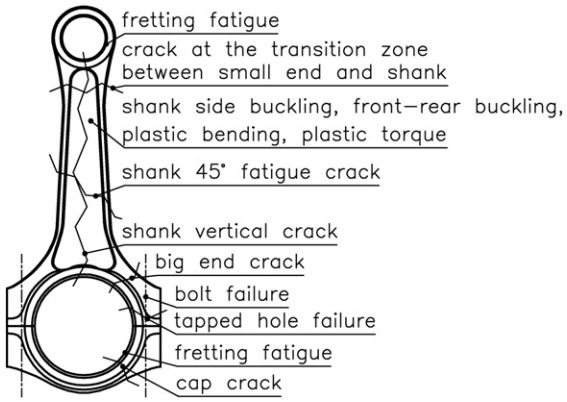

Fig. 1. The locations of the most critical con-rod sections.

of the various failures in terms of their stress field. The interpretation of the various collapses either rests on approximate formulae for the stress field, available in standard textbooks, see [5–10], or on more advanced theories, which will be recalled throughout the text where pertinent, or, finally, on FE forecasts.

To correctly interpret the con-rod fracture modes, it is necessary to understand the loads applied to this mechanical component. The following Sections separately address the various parts composing the con-rod, namely the shank and the small and big ends; their loading conditions and stress field are considered, and common and uncommon failure modes are discussed. The locations of the most critical con-rod sections examined throughout the paper are summarized in Fig. 1.

The collapsed con-rods illustrated in this paper form part of the collection of the Engineering Department Enzo Ferrari, Modena, Italy; the con-rods mainly originate from a long-lasting collaboration of the Engineering Department with several vehicle industries of the territory; the con-rods also constitute a teaching support to the courses offered on the structural design of internal combustion engine components.

2. Con-rod shank

The con-rod shank is subjected to compression, due to the combustion pressure, at top dead centre at the beginning of expansion, or when it is at bottom dead centre. Conversely, the shank undergoes tension, due to the inertial forces exerted by the mass of the piston and of the gudgeon pin, at top dead centre at the beginning of induction stroke. The fatigue stresses within the con-rod shank are therefore reversed.

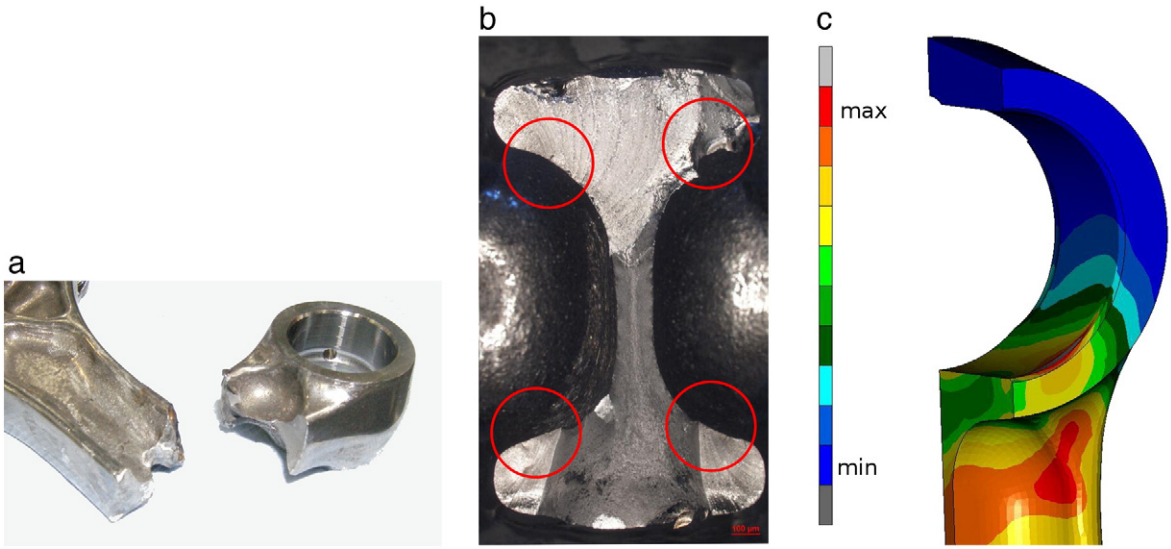

Fig. 2. Fatigue crack at the transition zone between the small end and the shank: (a) fatigue fracture; (b) crack initiation points; (c) FE forecasts: equivalent von Mises stress distribution.

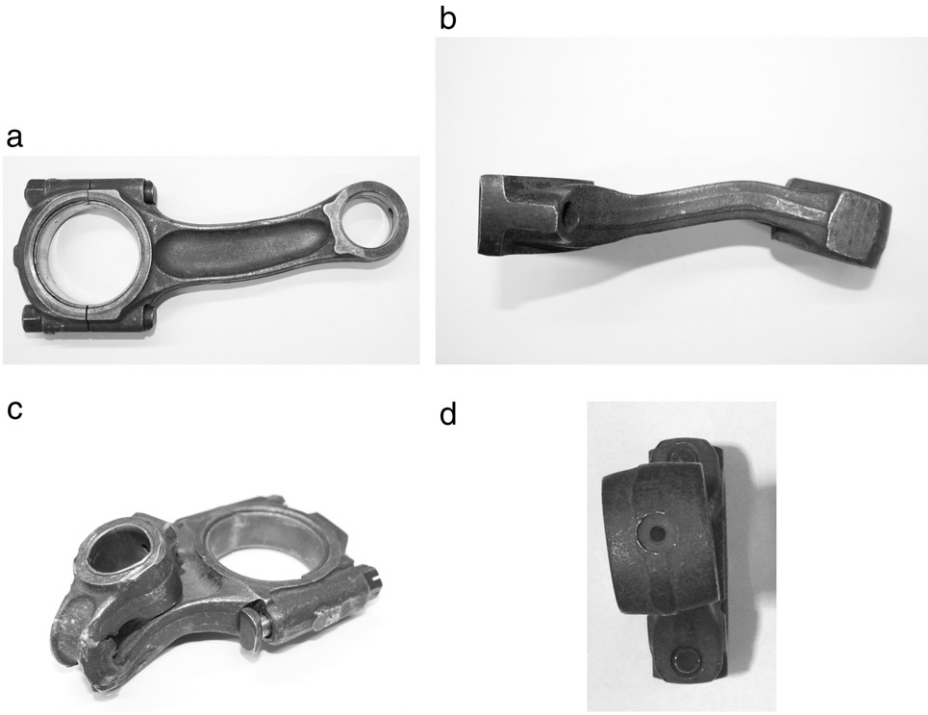

Fig. 3. Euler-type collapse of connecting rods: (a) side buckling; (b) front–rear buckling; (c) catastrophic buckling and (d) plastic torque.

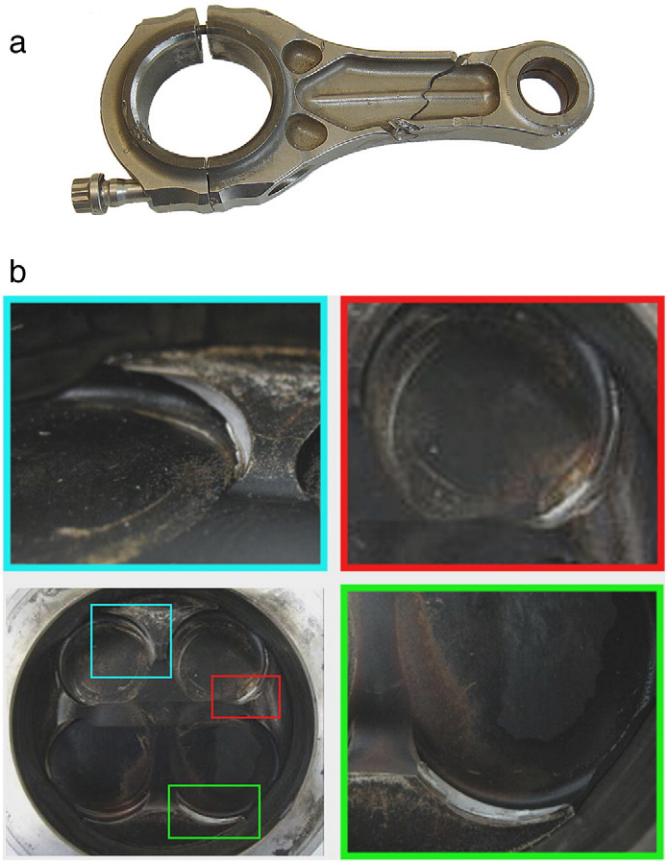

Fig. 4. Unusual 45° fatigue crack in the con-rod shank (a); contact between the piston and the valves due to torsional deflection of the con-rod (b).

The compression force due to combustion pressure, and the inertial tensile force, may be estimated with traditional approaches, *e.g.* [5–11]. Fig. 2(a) displays a common fatigue crack at the transition zone between the small end and the shank, see Fig. 1. In particular, Fig. 2(b) shows four crack initiation points, thus evidencing that the normal load is mainly responsible for this fatigue fracture. Fig. 2(c) shows FE forecasts of the equivalent von Mises stress distribution at top dead centre at the beginning of expansion. There is a perfect match between the maximum stress value location and the crack initiation points. Figs. 1 and 2 of [12] address a similar fatigue failure at the transition zone between the shank and the big end.

Since the geometries of both the small end and the big end on one side, and the shank on the other side, are considerably different, the first two structures being rings, whereas the second structure being a beam, their stresses do not easily match, and this difficulty in stress blending justifies the onset of stress concentrations, *e.g.* [9]. A FE study of the con-rod shank and, especially, of the transition zone between small end and shank is reported in [1,13] and a numerical analysis of the influence of fillets adopted in this area is presented in [14]. In [15,16] an optimization of the transition geometry between the shank and the big end is addressed. In [17,18] various shank failures at different positions are reported.

In addition to the above ordinary loading conditions, the con-rod may collapse as a result of an excessive compression force, see Figs. 1 and 3(a) and (b).

This situation usually occurs when the piston stroke is blocked by an engine seizure or when leaking coolant enters the combustion chamber. Such failure modes are often referred to as Euler-type collapse, although the collapse of Fig. 3 is elastic-plastic, whereas the Euler theory is purely elastic. In particular, Fig. 3(a) shows a side buckling of the con-rod shank, whereas Fig. 3(b) presents a front–rear buckling. In [19,20] both analytical and experimental results on con-rod buckling failures are illustrated. Fig. 3(c) displays a catastrophic buckling of a con-rod. The shank has been plastically bent up to a complete folding, as a result of the global collapse of the engine. Fig. 1 of [21] presents a similarly bent con-rod. Fig. 3(d) shows a con-rod subjected to

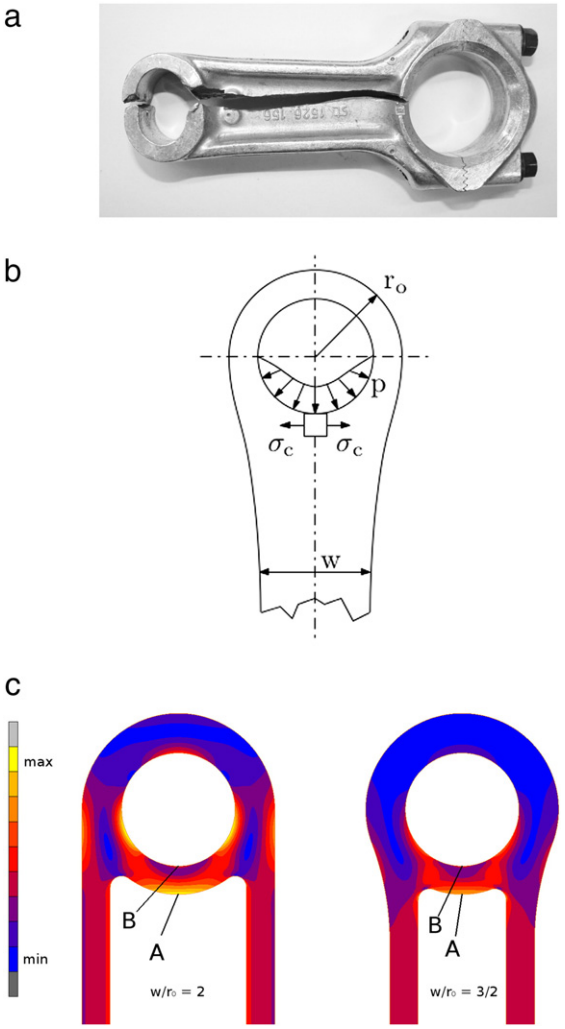

Fig. 5. Unusual failure in an aluminium con-rod: (a) influence of the w/r_0 ratio on the stress induced in the con-rod small end; (b) tensile stresses σ_c in the circumferential direction; (c) FE forecasts, equivalent von Mises stress distribution.

plastic torque, whereas bending yielding is not appreciable. This is an unusual failure mode, since it is difficult to imagine which plausible loading produces essentially torque without simultaneously provoking bending. The presented plastic torque of the con-rod might be explained by supposing a damage of the piston skirt or of the liner, and a consequent misalignment of the reaction force between the piston and the liner with respect to the moving plane of the con-rod.

Fig. 4(a) depicts a collapsed racing engine con-rod. The unusual 45° fatigue crack in the shank, see also Fig. 1, may be attributed to torsional vibrations and to resonance conditions, which may occur for critical angular speeds as high as 18,000 rpm, [22]. In this case, the excitation source of the system may be related to the torsional deflection of the crankshaft, which produces a misalignment between the axis of the rod journal and the main journal, [23]. The onset of torsional vibrations in the con-rod assembly may cause undesired impacts between the piston and the valve plate peripheries, see Fig. 4(b).

Fig. 5(a) shows an unusual fatigue failure in an aluminium con-rod, see also Fig. 1, in which the compression forces have vertically cracked the shank, thus splitting the whole con-rod into two parts.

It is noted that in Fig. 5(a) the geometry of the eye-shank transition zone is not traditional, since the shank sides are tangent to the small end periphery, see Fig. 6(d) of [24], whereas the classical proportions require that the ratio between the shank width, w, and the small end outer radius, r_0, ranges between 3/2 and 4/3, [24].

The compression between the small end and the piston pin produces appreciable compressive stresses caused by the contact pressure along the mating surfaces; as a result of this unusual geometry, this compression induces high tensile stresses σ_c in the circumferential direction, Fig. 5(b). Fig. 5(c) presents plane FE forecasts for two geometries exhibiting different w/r_0 ratios, namely $w/r_0 = 2$ and $w/r_0 = 3/2$.

The increase of the shank deformability exerted by the pocket has qualitatively been modelled by completely removing the corresponding material, see [25], in order to mimic a con-rod section laterally offset with respect to the con-rod symmetry plane perpendicular to the eye axes. For the two geometries examined, the hoop stresses at the points A and B are all tensile; the stresses at the points B are similar for the two cases, whereas the stresses at the points A are considerably higher for the geometry with $w/r_0 = 2$, thus confirming that the geometry of Fig. 5(a) should be avoided.

The con-rod shank may be either I-shaped (the shank pockets are frontal) or H-shaped (the pockets are lateral). In Formula 1, con-rods with both frontal and lateral pockets are currently employed. In [26], p. 488, the two geometries are compared under various aspects. In this paper, the influence is particularly addressed of the two geometries on the intensity of the lateral pressure peaks at the contact between gudgeon pin and small end bore, see Fig. 6.

The pin is deflected by the combustion forces exerted by the piston bosses, and this bending promotes high contact stresses at the pin-eye contact ends. If the shank is I-shaped, the presence of the pockets increases the deformability of the shank projecting zones sustaining the gudgeon pin. Since these projecting zones are sufficiently deformable, the contact pressure remains reasonably uniform in the axial direction, and the lateral contact pressure peaks are limited. Instead, if the shank is H-shaped, the shank

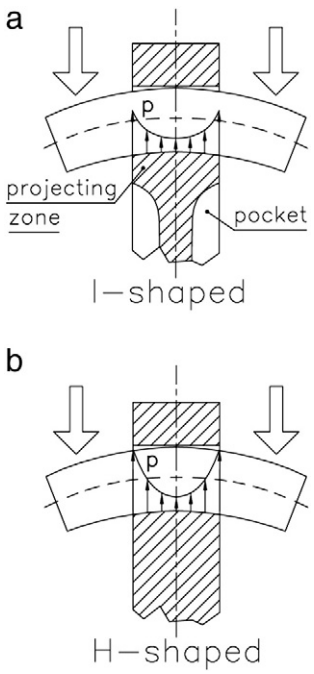

Fig. 6. Influence of the shank geometries on pressure peaks at the contact between gudgeon pin and small end bore: (a) I-shaped shank; (b) H-shaped shank.

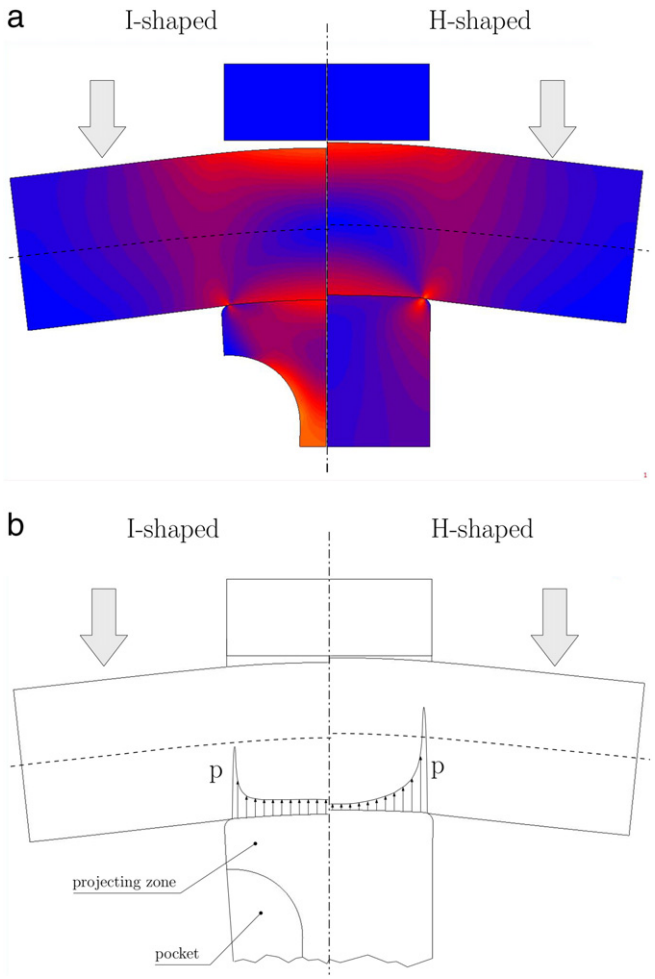

Fig. 7. Plane FE analysis of the contact pressure between gudgeon pin and small end: (a) equivalent von Mises stress distribution; (b) contact pressure distribution.

zones supporting the gudgeon pin are less flexible, so that the contact pressure is not uniform, and the lateral contact pressure peaks are higher.

Fig. 7 shows a plane FE analysis of the contact between gudgeon pin and small end, in the presence (*I*-shaped) or in the absence (*H*-shaped) of the pocket. An appreciable decrease of the lateral contact pressure peaks is registered for the *I*-shaped configuration, the total contact force being the same for the two cases.

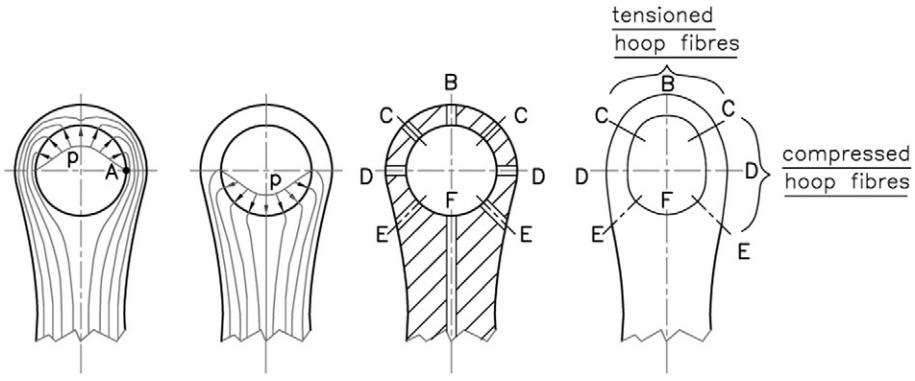

Fig. 8. Peculiarity of the con-rod small end: (a) stress flow for a tensile force; (b) stress flow for a compressive force; (c) possible positions of the lubrication hole; (d) circumferential strains and stresses along the periphery hoop.

In some high performance *H*-shaped con-rods, a small frontal pocket is added to increase the deformability of the shank zones supporting the gudgeon pin, see Fig. 13(b) below.

3. Con-rod small end

Moving to the small and big ends, they remain virtually undistorted when the con-rod is subjected to compression at top dead centre at the beginning of expansion, or when it is at bottom dead centre, since in both these stroke positions the gudgeon pin or the crankpin compress the small or big ends along arcs of their bores that are adjacent to the shank, so that the compression load directly transfers to the con-rod shank without significantly stressing the two eyes. Conversely, the two eyes are appreciably loaded at top dead centre at the beginning of induction stroke, by the tensile inertial forces exerted by the mass of the piston and of the gudgeon pin. The fatigue stresses within the con-rod eyes are therefore repeated, *e.g.* [8].

In [27] the approximate formulae are reviewed that are available for predicting the stresses in a small end; they constitute a basis for the interpretation of the small end failures.

Figs. 8(a) and (b) qualitatively show the stress flow within the small end, promoted by the contact pressure p with the gudgeon pin. In particular, Fig. 8(a) represents the stress flow at top dead centre at the beginning of induction stroke, when the gudgeon pin pushes the small end along a contact arc that is not adjacent to the shank. The small end is heavily stressed, and the stress maximum falls in the point *A*, *i.e.* at the small end bore sides. On the contrary, Fig. 8(b) depicts the situation at top dead centre at the beginning of expansion, or at bottom dead centre. In these cases the contact arc between pin and small end is adjacent to the shank, and the small end is virtually unloaded.

Fig. 9(a) presents the plane photoelastic stresses within the small end for a tensile force. It shows that tensile forces activate high stresses within the whole eye, and it confirms that the maximum stresses occur at the eye bore sides. The 3D FE forecasts of Fig. 9(b) validate the photoelastic measurements.

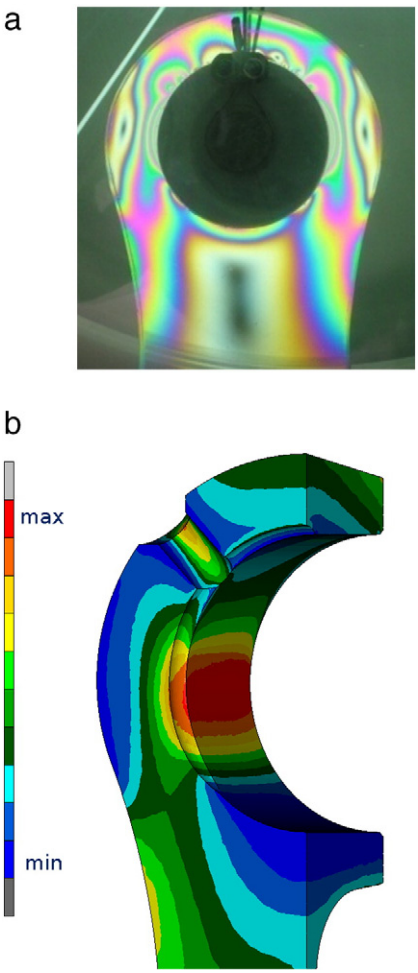

Fig. 9. Stresses distribution within the small end for a tensile force: (a) plane photoelastic measurement; (b) 3D FE forecasts, max. Principal stress distribution.

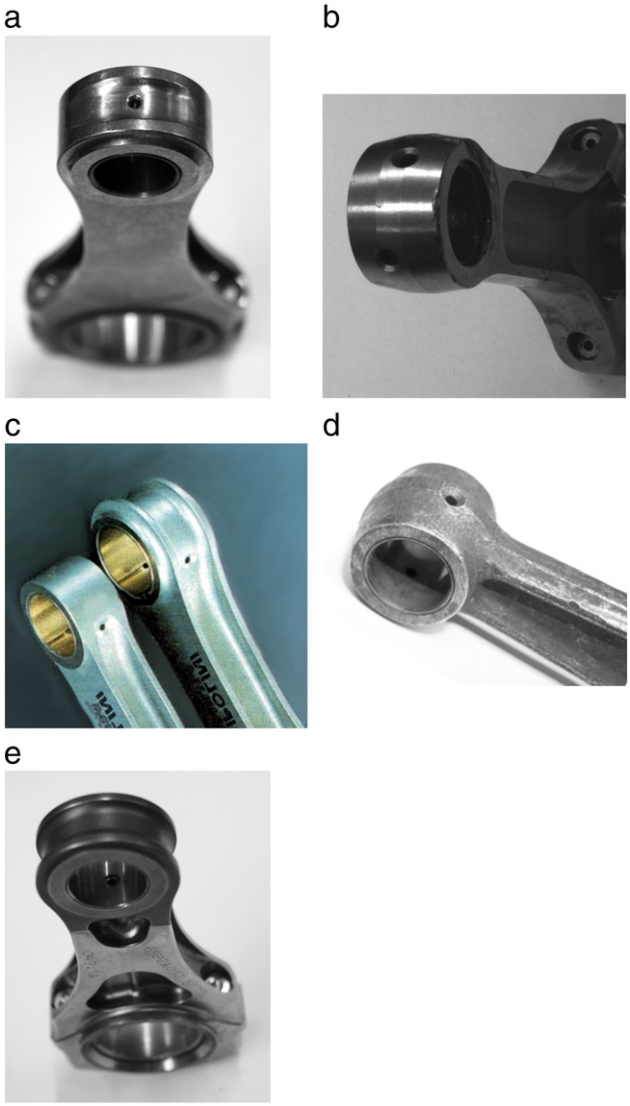

Fig. 10. Possible location of the lubrication hole in the con-rod small end: (a) 0° location; (b) 45° location; (c) 135° location; (d) 90° location; (e) 180° location from the vertical axis of the con-rod.

Fig. 8(c) collects various positions of the lubrication hole; the most favourable positions will be discussed according to the stress distribution. The position *B* constitutes the most traditional solution, see Fig. 10(a). The positions *C* and *E* are justified by the ovalization of the small end at the beginning of induction stroke, which is characterized by the circumferential strains and stresses along the periphery hoop fibres changing their sign, and, therefore, becoming null, in the vicinity of the four points *C* and *E*, Fig. 8(d) and [28]. To locate the lubrication holes in such virtually unloaded zones avoids the onset of stress concentrations, see Fig. 10(b) and (c). The duct in *F* collects the pressurized lubricant from the crankshaft. The zone *D*, at the small end bore sides, is characterized by high stresses, see Fig. 8(a), and, therefore, the lubrication hole should not be placed in this zone. Fig. 10(d) presents an inexplicable exception to this rule.

Although the approximate formulae available in the pertinent literature for predicting the stresses in a small end, [27], are currently employed for a preliminary design of the small ends, they do not account for the effect of the initial clearance between the eye bore and the gudgeon pin periphery. This aspect is examined in the following Section. Another difficult problem is the selection of the correct interference between eye and bush, that prevents an undesired bush loosening; this aspect will be examined in Section 3.2. Finally, Section 3.3 will address fretting fatigue failures at the con-rod small end.

3.1. Effect of the initial clearance between small end bore and pin periphery

To avoid seizure, a clearance is introduced between the small end bore and the gudgeon pin. The initial diametral clearance generally falls within the interval 0.0008–0.003 times the pin radius, [24].

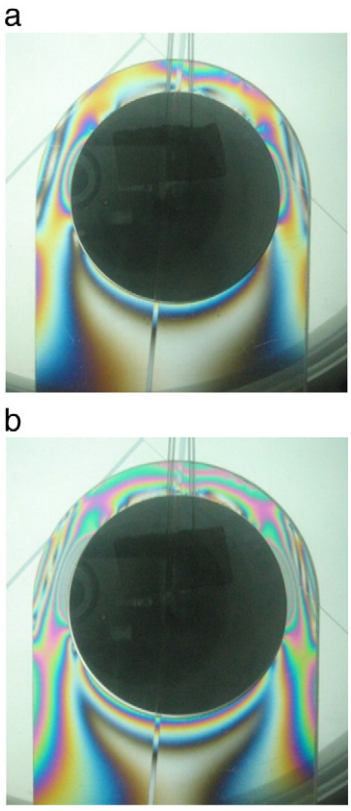

Fig. 11. Photoelastic analysis of a pin-lug connection: (a) applied load equal to 196.2 N and initial diametrical clearance equal to 0.5 mm; (b) applied load equal to 392.4 N and initial diametrical clearance equal to 1.0 mm.

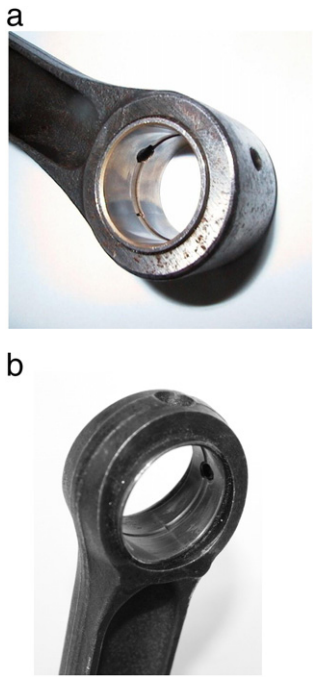

Fig. 12. Undesired rotation of the bush forced into the small end: (a) standard small end geometry; (b) small end with a viper head shape.

This contact is classified as progressive, since the contact extent increases with the applied load. This contact problem is therefore nonlinear, and, consequently, it is a computationally demanding task to prepare diagrams reporting the increase in the eye stress, with respect to a neat fit reference configuration, for a variety of combinations of applied loads and initial clearances.

A breakthrough has been achieved in [29] dealing with a pin inserted into a hole drilled in an infinite plate, in the presence of initial clearance. This geometry resembles the contact between the small end and the gudgeon pin. It has been shown that the extent of the contact arc depends on the ratio between load and clearance; consequently, the above ratio may be treated as a single variable. In addition, in two geometries for which the above ratio is the same, the stress pattern remains the same.

In [30] it has been shown that the above properties hold for plates of finite dimension too. The pin-lug connection and the pin-eye contact belong to this category.

A photoelastic analysis has specifically been carried out to validate the above analytical forecast. Two pin-lug connections of equal nominal geometry have been considered, Fig. 11. The load applied to the first connection is 196.2 N, and the initial diametrical clearance is 0.5 mm, Fig. 11(a); the load of the second connection is 392.4 N, and the initial diametrical clearance is 1.0 mm, Fig. 11(b); the ratio between load and clearance is the same for the two cases. Encouragingly, the photoelastic patterns of Fig. 11(a) and (b) are very similar.

It has previously been observed that the extent of the contact arc depends on the ratio between the load and the clearance, rather than on their single values. Having reduced by one the number of independent variables, it becomes conceivable to compile diagrams reporting the stress concentration *versus* the ratio between load and clearance, for a variety of small end geometries. These design diagrams have been prepared in [24] (see also [31]). Each diagram holds for particular inner to outer radii ratios for the con-rod small end and for the gudgeon pin. In addition, the *x*-axis of each diagram reports a load factor, see [29–30] that summarizes the combined effect of the tensile load applied to the con-rod, the initial radial clearance, and the Young's modulus. These diagrams allow the small end stress increase due to the presence of an initial clearance to be estimated with respect to the reference situation of initial neat fit.

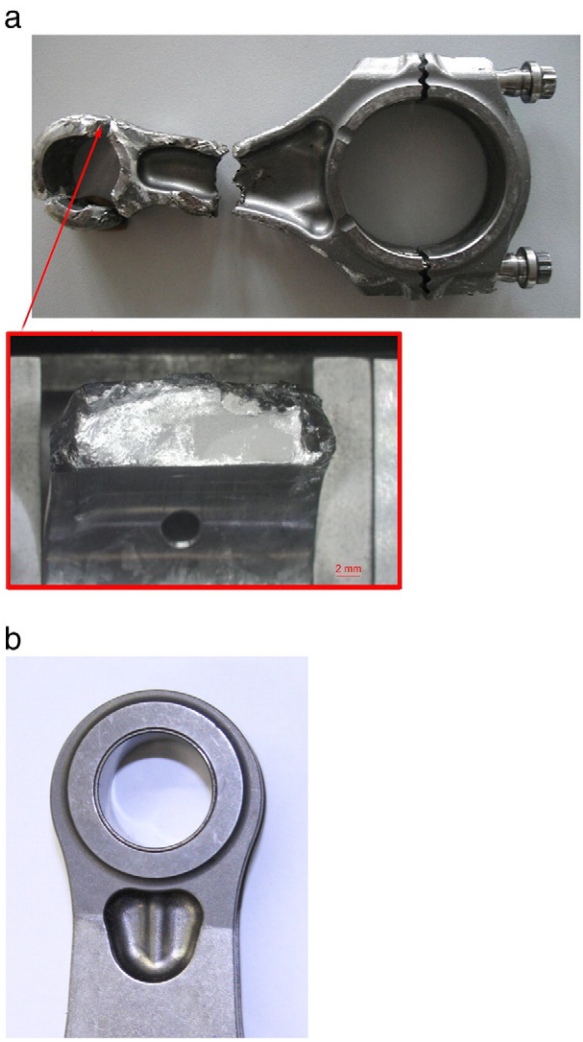

Fig. 13. Fretting in con-rod small end: (a) fatigue crack in con-rod small end; (b) titanium con-rod small end with DLC anti-fretting coating.

As an example, in [24] a steel small end defined by an outer radius of 18 mm and by an inner radius of 10 mm is considered. The gudgeon pin is defined by an outer radius of 10 mm and by an inner radius of 5 mm. The initial radial clearance is 0.01 mm and the total tensile load is 7875 N. With the aid of the design charts, the increase in eye hoop stress attributable to the initial clearance, with respect to a neat fit, was found to be 22%.

3.2. Bush loosening

Fig. 12 illustrates an undesired rotation of the bush forced into the small end. As a result of this rotation, the lubrication hole is obstructed. Consequently, the contact between small end and gudgeon pin is no longer lubricated, and seizure generally occurs, which causes the failure of the piston–pin assembly. It is noted that in Fig. 12(b) the small end exhibits a viper head shape, which is more commonly employed in diesel engines.

In [32] a modelling is developed that expresses the analytical connection between the bush-eye initial interference and the bush loosening force. This piece of information permits the designer to select the bush-eye interference according to sound engineering judgement and not only to his personal experience. In [32] it is assumed that eye-bush loosening occurs when the tensile inertial force acting at top dead centre at the beginning of the induction stroke elongates the length of the eye bore border, until it

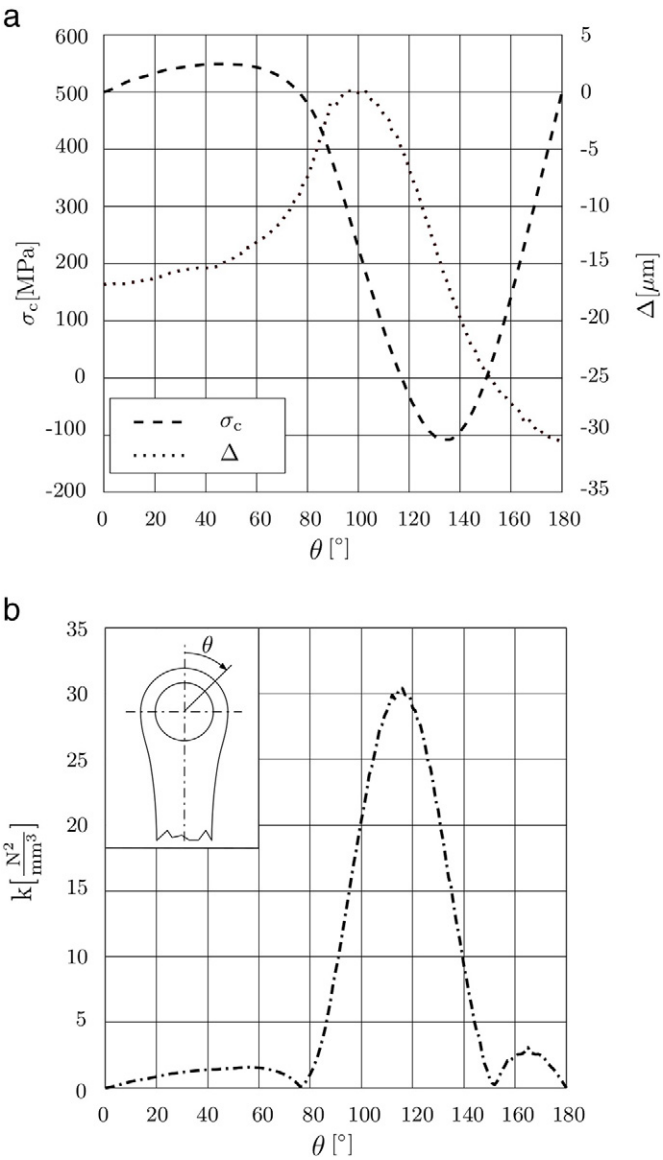

Fig. 14. Parameters used to describe fretting fatigue: (a) circumferential stress distribution, σ_c, and relative tangential displacement amplitude, Δ, between con-rod and bush; (b) fretting fatigue distribution according to Ruiz criterion along the con-rod small end bore.

equals the initial length of the bush periphery, see Fig. 2 of [32,33]. In this situation the contact pressure becomes virtually null, and bush rotation may occur.

In the absence of a significant torque applied to the bush, the causes of the bush rotation are unclear, and they have tentatively been attributed to vibration effects or to cumulative microslip phenomena, see *e.g.* [32,34,35].

3.3. Fretting fatigue damage in small ends

The microslip between the bush and the small end may produce fretting fatigue cracks, see Fig.1. Fig. 13(a) reproduces a fretting fatigue crack occurring in a small end.

Fig. 14 shows the parameters used to describe the fretting fatigue along the con-rod small end bore, with reference to the titanium con-rod of Fig. 13(a). The maximum tensile inertial load applied to the assembly is 40,000 N, the small-end inner and outer diameters are 24 mm and 36 mm, respectively, whereas the axial thickness is 21 mm. In particular, Fig. 14(a) displays the maximum circumferential stress along the small end bore, at top dead centre at the beginning of the induction stroke, as well as the relative tangential displacement amplitude, Δ, between the con-rod and the bush during a complete engine cycle. The origin of the angular coordinate coincides with the top point of the eye bore, see the inset of Fig. 14(b).

The circumferential stress distribution, σ_c, is consistent with Fig. 9, since it exhibits a maximum value around 100°. However, the section defined by 100° rarely collapses; instead, the commonly encountered collapse occurs at about 135°, see Fig. 13(a) and [36]. Therefore, a purely stress based parameter has to be abandoned in favour of an alternative interpretation of the failure mechanism in terms of fretting fatigue. In fact, *i*) for the case of Fig. 14, the absolute value of the maximum relative displacement (30 μm) agrees with the range (10–40 μm) reported in [37] as a minimum fretting-fatigue life indicator; *ii*) the maximum of the fretting fatigue parameter proposed by Ruiz [38] occurs at an angle of approximately 125°, which coincides with the experimentally detected crack position of Fig 13(a).

The Ruiz parameter, *k*, [38] is:

$$k = \sigma_c \cdot \Delta \cdot p \cdot f \tag{1}$$

where σ_c is circumferential stress, Δ is the relative tangential displacement amplitude displacement, *p* is the pressure distribution between the con-rod small end and the bush and, finally, *f* is the friction coefficient assumed to be equal to 0.1 in these calculations. Methods to lower the fretting parameter are presented in [39,40].

In titanium con-rods, such as those of Fig. 13, the fretting phenomena may be so strong that the con-rod small end has to be coated with proper anti-friction coatings (DLC) to minimize the friction coefficient between the small end and the bush, see Fig. 13(b).

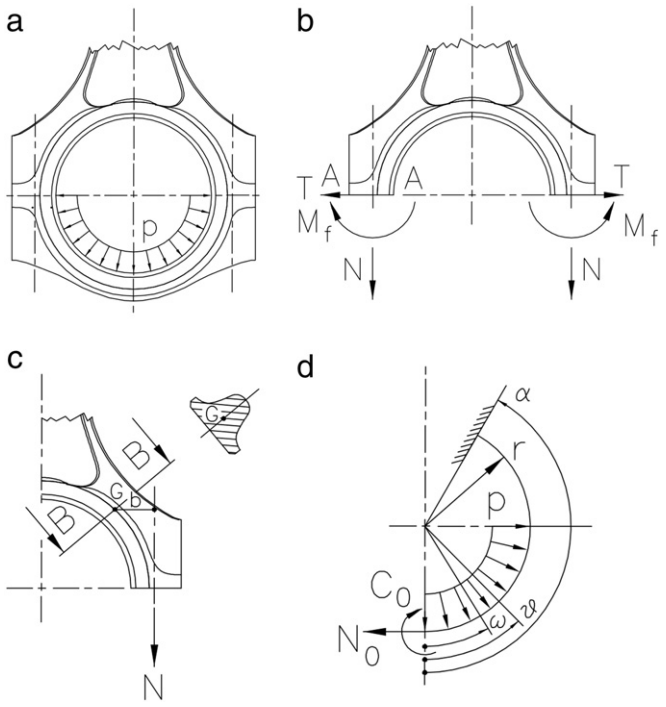

Fig. 15. Mechanical behaviour of the area connecting the shank and the big end: (a) external loadings; (b) complete model; (c) simplified model; (d) analytical model.

4. Con-rod big end

Two main architectures are available of the con-rod big end, depending on the peculiar crankshaft con-rod assembly. In fact, if the crankshaft is manufactured in different parts, the con-rod can be produced as a monolithic component. In this case, the geometry of the con-rod big end is quite similar to the con-rod small end, and almost the same considerations presented in the previous sections hold, *e.g.* [16]. On the other side, if the crankshaft is manufactured in a single part, the con-rod big end has to be split into two separate components, namely the con-rod and the cap, joined by a bolt connection. In this case, a more complex mechanical behaviour of the assembly occurs, and different failure mechanisms may arise. In the following, failures of the critical area connecting the shank and the big end, of the bolt connection, and of the critical cross-sections of the cap, are investigated. Moreover, possible fretting damages are discussed.

4.1. Connecting area between the shank and the big end

The evaluation of the loading of the area connecting the shank and the big end, see Fig. 1, is treated in standard textbooks, *e.g.* [5–10]; a load analysis is perfunctorily presented in the following. Fig. 15(a) addresses the big end loading.

In particular, the forces N transmitted by the bolts act simultaneously with the bending moments, M_f and the shear forces, T, both the rotation, and the radial shift of the extremity A–A being hindered by the presence of the cap, Fig. 15(b). The shear force, T, is usually assumed not to be relevant because of the reasonable symmetry of the big end with respect to a horizontal axis, whereas the bending moment, M_f, is neglected because this assumption is conservative. Consequently, the maximum bending moment, falling along the section B–B, may be estimated by considering only $N = p \times r$. In Fig. 15(c), b denotes the lever of the force N.

It was decided to assess these approximations, by modelling the big end as an incomplete ring of uniform cross section, clamped to the shank at an angle $\alpha = 150°$, and loaded by a uniform pressure p, see Fig. 15(d). It was found that the shear

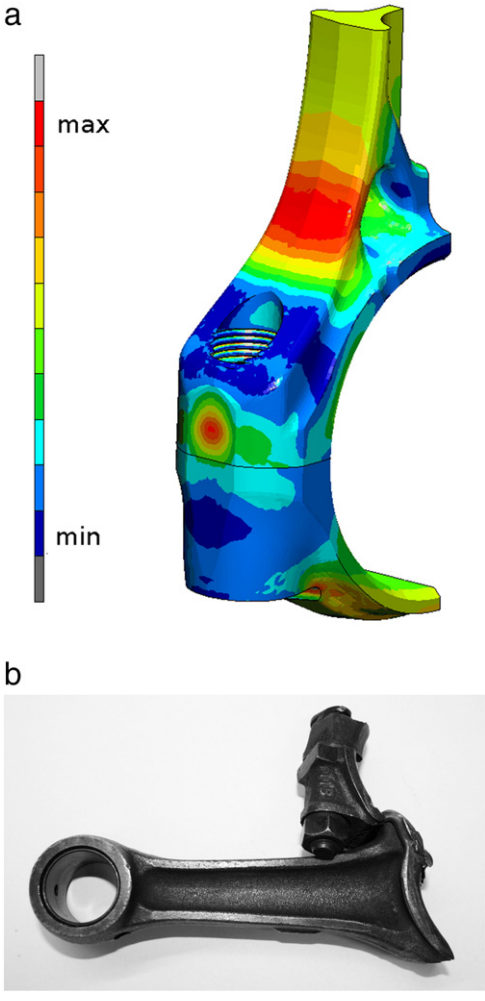

Fig. 16. FE analysis of the stress field within a con-rod big end: distribution of the maximum principal value of stress (a); fracture in con-rod big end (b).

force at the transition section between the big end and the cup, defined by the angular position $\theta = \pi/2$, is only 16% times the normal force N. To examine the relative importance of the bending moment M_f evaluated for $\theta = \pi/2$, it is observed that the lever b is of the order of 0.5 times the radius r. The bending moment M_f computed for $\theta = \pi/2$ is about 20% of the bending moment evaluated in the section B–B and due to N alone. Moreover, M_f is of opposite sign with respect to the bending due to N alone, and, therefore, it is conservative to neglect it, Fig. 15(c).

The VDI standards 2230 [41] report some additional observations on the connection between shear forces and frictional coefficient in the big end.

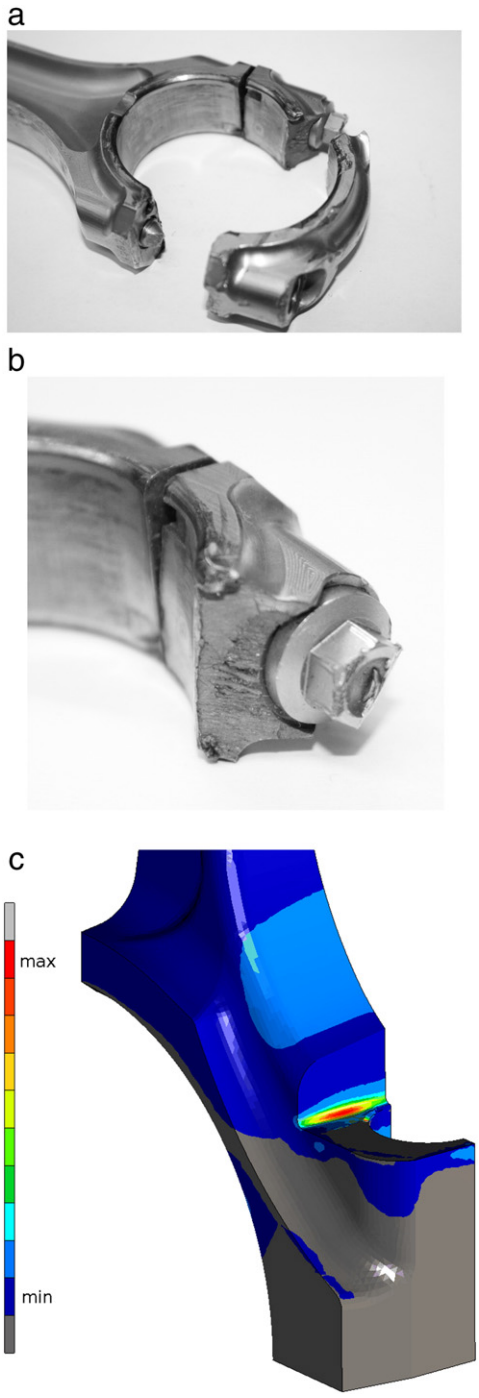

Fig. 17. Failure of the bolt connection: fatigue crack in the cap: (a) global; (b) detail; (c) undesired stress concentrations in the big-end induced by through screws: maximum principal stress distribution.

Fig. 16(a) presents a FE analysis of the stress field within a big end. In particular, the maximum principal value of stress is reported at the top dead centre at the beginning of the induction stroke. The stresses are particularly high at the big end zone adjacent to the shank where the cross section is minimal.

Fig. 16(b) illustrates a typical fracture in the big end. This fracture is similar to that of Figs. 26 and 27 of [42], Fig. 2 of [43] and Fig. 19 of [28].

4.2. Bolt connection

Both through screws and cap screws with the tapped hole machined in the con-rod are usually employed to connect the big end and the cap. Whatever the particular topology adopted, cracks may be registered in the con-rod, see Fig. 3 of [44], in the cap, see Figs. 17(a) and (b), or in the bolt, see Fig. 18, Fig. 1 of [43], Fig. 3 of [45], and also Fig. 1. Nevertheless, cap screws are usually preferred when the inertial forces are particularly high. In fact, if through screws are adopted, the big end has to be machined to house the bolt head, and this shape induces undesired stress concentrations in the critical area connecting the con-rod and the big end, see Fig. 17(c). FE studies addressing the bolt connection are reported in [46,47].

4.3. Big end cap

Fig. 19 collects three cross sections employed for the cap. Cross section (I), characterized by a single central rib, is the commonest geometry, since it may be formed. Section (II) adopts two lateral ribs, which better house the head of the screw, thus reducing stress concentrations. Section (III) has been proposed recently. It employs two lateral pockets, which confer some desired radial deformability to the cap, thus making the contact pressure more even, and reducing the end pressure peaks in the crankpin axial direction between the big end and the crankpin, see the similarity with Fig. 6 and [16].

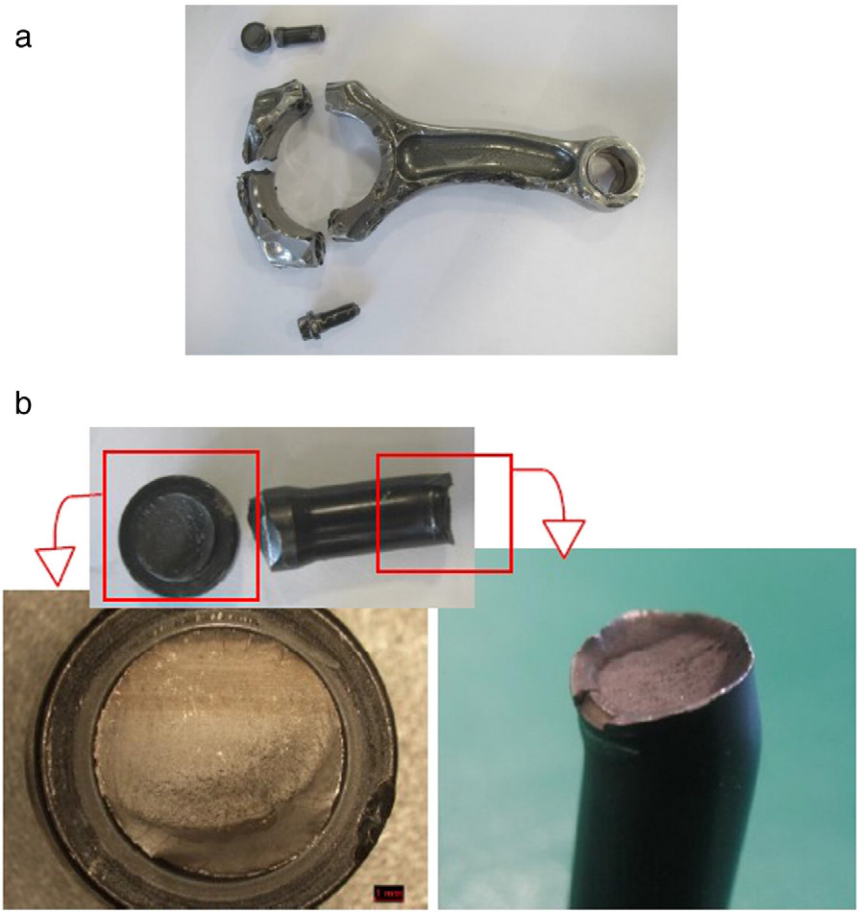

Fig. 18. Fatigue crack in the bolt:(a) global view; (b) bolt detail.

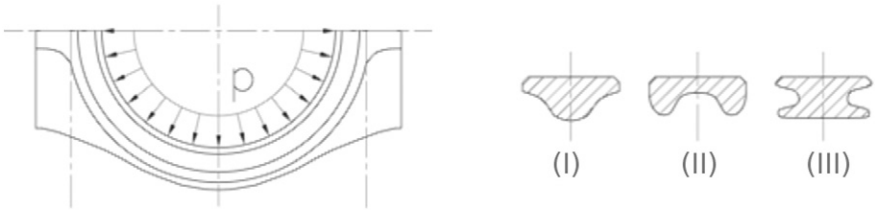

Fig. 19. Three cross sections employed for the cap.

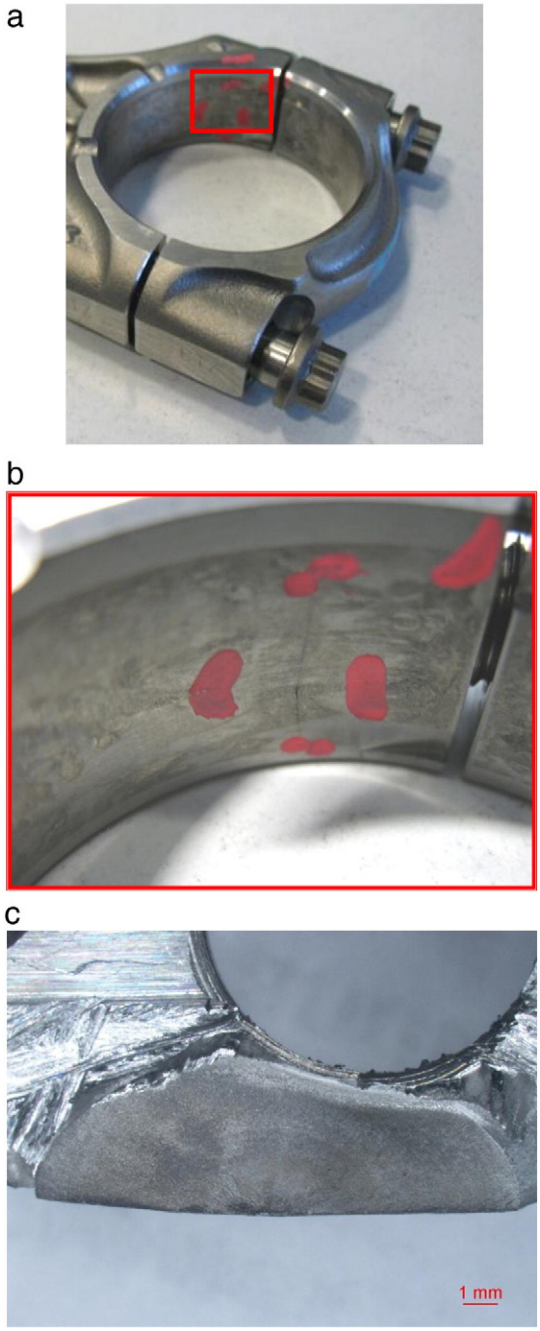

Fig. 20. Fretting fatigue crack propagating from the big end inner border: (a) global view; (b) detailed view; (c) fracture section.

4.4. Fretting fatigue damage in big ends

It should be observed that in the approximate analytical approach of Fig. 15 the maximum tensile stress occurs along the big end periphery, thus suggesting that the fatigue crack should nucleate from this zone, *e.g.* Figs. 26 and 27 of [42]. Nevertheless, fatigue cracks have been observed that propagate from the big end inner border, see Fig. 1. This fatigue damage may be rationalized in terms of fretting fatigue, connected to the lateral micro-movements of the big end with respect to the bearing, *e.g.* [48]. Fig. 20 evidences the fretting fatigue crack propagating from the big end inner border.

Fig. 21 shows the parameters used to describe the fretting fatigue along the con-rod big end bore, with reference to the titanium con-rod of Fig. 20. The maximum tensile inertial load applied to the assembly is 65,000 N, the big-end inner and outer diameters are 50 mm and 60 mm, respectively, whereas the axial thickness is 22 mm. In particular, Fig 21(a) displays the maximum circumferential stress along the big end bore, at top dead centre at the beginning of the induction stroke, as well as the relative tangential displacement amplitude, Δ, between the con-rod and the bearing during a complete engine cycle. The origin of the angular coordinate coincides with the lateral point of the big-end bore, see the inset of Fig. 21(b).

Similar to the above presented small end, *i*) for the case of Fig. 20, the absolute value of the maximum relative displacement (37 μm) agrees with the range (10–40 μm) indicated in [37] as a minimum fretting-fatigue life indicator; *ii*) the maximum of the

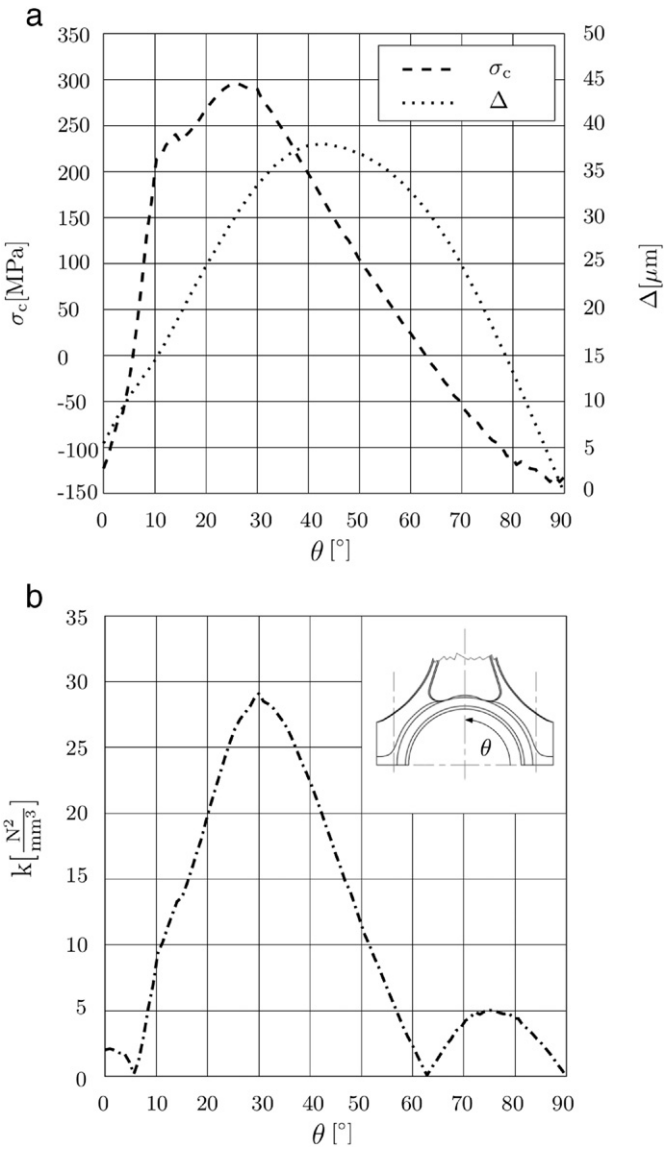

Fig. 21. Parameters used to describe fretting fatigue: (a) circumferential stress distribution, σ_c, and relative tangential displacement amplitude, Δ, between con-rod big end and bearing; (b) fretting fatigue distribution according to Ruiz criterion along the con-rod big end bore.

fretting fatigue parameter proposed by Ruiz [38] occurs at an angle of approximately 30°, which coincides with the experimentally detected crack of Fig. 20, thus supporting the fretting fatigue interpretation.

Analogous fretting failures may be registered in the cap, see Fig. 1 and Fig. 1 of [49].

5. Tribological aspects

The present paper mainly addresses different fracture mechanisms affecting the critical areas of a connecting rod. Nevertheless, additional phenomena may induce the failure of the assembly such as those involving tribological aspects in the con-rod big end and small end bearings. This section briefly describes some of these aspects; the interested reader may refer to the pertinent literature, *e.g.* [50], for further details.

The way the hydrodynamic lubrication process sustains the external load in the con-rod big end and in the small end counterpart is strongly different [51]. In fact, in the con-rod big end, the fluid film formation is mainly guaranteed by the high rotational speed between the rod and the crankshaft. The relative speed between the two lubricated profiles forms a wedge of fluid that ensures the appropriate lubrication, thus avoiding undesired direct contacts. On the contrary, at the con-rod small end, the relative speed is low, and a complete rotation between the mating surfaces does not occur since the con-rod only

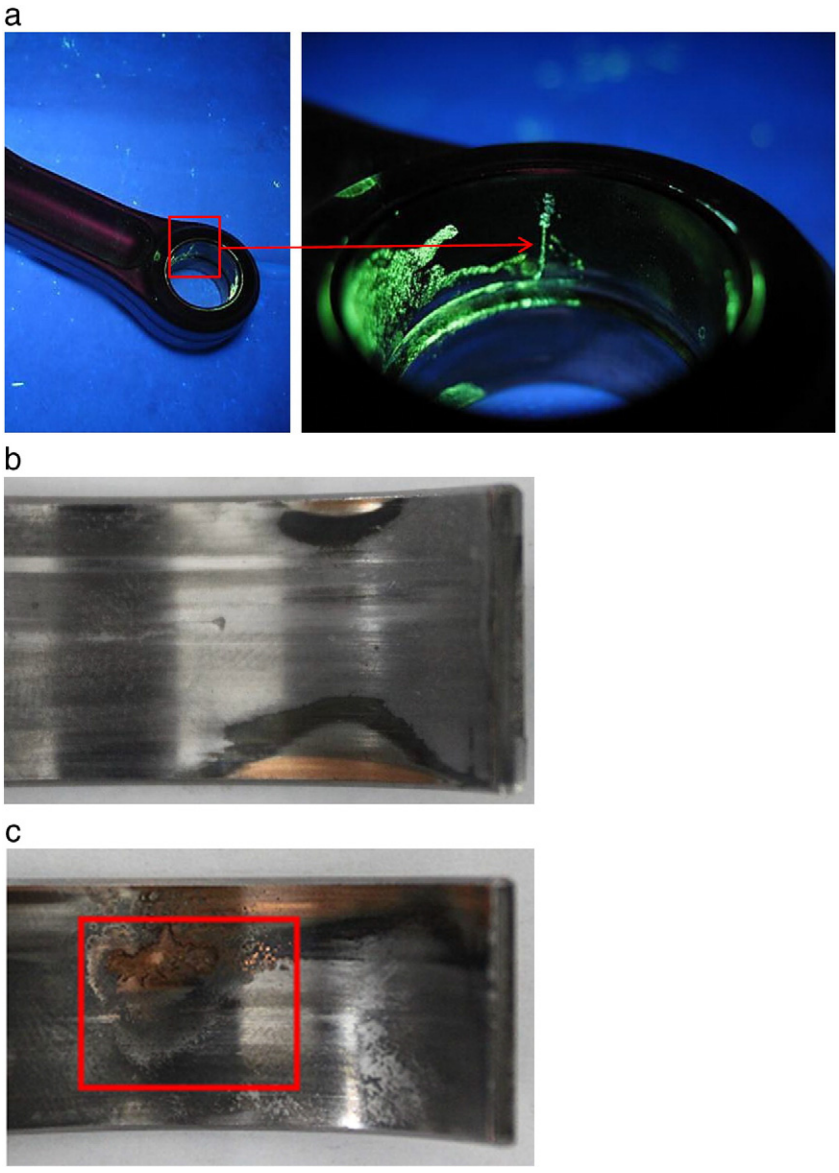

Fig. 22. Tribological types of damage: (a) wear damage in the con-rod small end bush, (b) wear damage in the big end bearing; (c) cavitation damage in the big end bearing.

oscillates around its vertical axis. Therefore, the dominant effect in the lubrication of the small end is the squeeze caused by the alternating high loads transmitted by the piston pin. Both combustion forces and inertial forces contribute to the squeeze effect.

To help the design engineers in avoiding undesired failures, see Figs. 22, it is fundamental to develop numerical methodologies for the analysis of the lubrication behaviour of these bearings.

The modelling of the lubrication mechanisms in the con-rod small end and big end has been the subject of various papers, *e.g.* [52–54]. In particular, a difficult aspect is the simulation of the lubricant cavitation in the zones where the pressure tends to become negative, and of the possible film reformation, *e.g.* [55,56].

Cavitation has to be properly modelled, since it might be directly responsible for the bearing damage [57], see Fig. 22(c). It has been shown that the cavitation problem may thoroughly be expressed in terms of complementarity, a relevant advantage being the fact that robust routines are available to numerically treat complementarity problems, [58,59]. This complementarity approach has recently been employed to detect the cavitated zones in the big end bearing in [60], and a good agreement has been achieved between computer simulations and bearing damaged zones.

6. Conclusions

Both typical and uncommon failure modes in con-rods for internal combustion engines have been commented from the stress level viewpoint. The interpretation of the fractures has been supported with traditional calculations, with more advanced analytical models, and with FE predictions. The locations of the most critical con-rod sections examined in this paper are summarized in Fig. 1.

With reference to the con-rod shank, the fatigue cracks occurring at the transition zone between the small end and the shank have been considered, and the corresponding stress concentrations have been illustrated with a FE analysis. Examples of side buckling, of front–rear buckling, and of plastic torque of the con-rod shank, have been presented, and their possible causes have been explored. The occurrence of an unusual 45° fatigue crack in the con-rod shank has been justified. An uncommon fatigue crack, splitting the whole con-rod into two parts, has been detailed, and the tensile stresses promoting such crack have been attributed to a non traditional geometry of the eye-shank transition zone. The influence of the *I*-shaped and *H*-shaped shank geometries on the pressure peaks at the contact between the gudgeon pin and the small end bore has been illustrated with FE.

Moving to the con-rod small end, both photoelastic and FE studies have been employed to evidence that the peak stress occurs at the small end bore sides. The possible positions of the lubrication hole have been classified. Recent analytical results on the effect of the initial clearance between the small end bore and the pin periphery on the small end stress field have been reported. According to these results, the extent of the contact arc between the small end and the gudgeon pin depends on the ratio between the load and the clearance; consequently, this ratio may be treated as a single variable. The validity of this analytical result has experimentally been assessed with a specific photoelastic analysis. The undesired rotation of the bush forced into the small end, causing obstruction of the lubrication hole and seizure, has been considered. The outcome of fretting fatigue cracks has been illustrated, and an output expressed in terms of the Ruiz fretting fatigue parameter has been provided for a specific titanium con-rod; this output justifies the crack initiation at the small end bore but not at the bores sides, where the maximum circumferential stresses occur.

Moving to the con-rod big end, a classical analytical model based upon several approximations has theoretically been assessed. A FE analysis has been carried out to evidence the noticeably high stresses at the big end zone adjacent to the shank, where the cross section is minimal. The employment of through screws has been shown to be particularly detrimental. The collapse of the big end cup and of the bolts employed to connect the big end to the cap, has been discussed. Fretting fatigue damage in the big end has been considered, and an output expressed in terms of the Ruiz fretting fatigue parameter has been provided for a specific titanium con-rod; this output justifies the crack initiation at the big end bore.

Moving to tribological aspects, the difference in the way the hydrodynamic lubrication process sustains the external load in the con-rod big end and in the small end counterpart has been underlined. The difficulties encountered in modelling the cavitation mechanism in lubricated contacts have been highlighted. The results have been reported of a numerical study exhibiting a good agreement between computer simulations and damaged zones of big end bearing.

References

[1] Y.M. Yoo, E.J. Haug, K.K. Choi, Shape optimal design of an engine connecting rod, J. Mech. Transm.-T ASME 106 (3) (1984) 415–419.
[2] R.J. Yang, D.L. Dewhirst, J.E. Allison, A. Lee, Shape optimization of connecting rod pin end using a generic model, Finite Elem. Anal. Des. 11 (3) (1992) 257–264.
[3] P.S. Shenoy, A. Fatemi, Connecting rod optimization for weight and cost reduction. No. 2005-01-0987, SAE Technical Paper, 2005.
[4] M.T. Lapp, R.A. Krause, C.C. Hall, D. Dinu, A. Antoc, Advanced connecting rod design for mass optimization. No. 2010-01-0420, SAE Technical Paper, 2010.
[5] R. Giovannozzi, Costruzione di Macchine, Patron Editrice, Bologna, 1965.
[6] V. Arkangelsky, M. Khovakh, Y. Stepanov, V. Trusov, M. Vikhert, A. Voinov, Motor Vehicle Engines, MIR, Moscow, 1971.
[7] A.I. Kolchin, V.P. Demidov, Design of Automotive Engines, MIR, Moscow, 1984.
[8] A. Garro, Progettazione Strutturale del Motore, Levrotto & Bella, Torino, 1992.
[9] A. Strozzi, Costruzione di Macchine, Pitagora, Bologna, 1998.
[10] D. Vignocchi, Elementi di Progettazione del Motore, Athena, Modena, 2002.
[11] P.S. Shenoy, A. Fatemi, Dynamic analysis of loads and stresses in connecting rods, Proc. Inst. Mech. Eng. C J. Mech. Eng. Sci. 220 (5) (2006) 615–624.
[12] M.N. Ilman, R.A. Barizy, Failure analysis and fatigue performance evaluation of a failed connecting rod of reciprocating air compressor, Eng. Fail. Anal. (2015).
[13] S. Athavale, P.R. Sajanpawar, Studies on some modelling aspects in the finite element analysis of small gasoline engine components. No. 911271, SAE Technical Paper, 1991.
[14] A. Mirehei, M.H. Zadeh, A. Jafari, M. Omid, Fatigue analysis of connecting rod of universal tractor through finite element method (ANSYS), J. Agric. Technol. 4 (2) (2008) 21–27.
[15] S.Y. Lee, S.B. Lee, H.S. Kim, T.G. Kim, M.G. Kam, J.W. Yoon, Failure analysis of connecting rod at big end, Key Eng. Mater. 306 (2006) 345–350.

[16] S. Khare, O.P. Singh, K.B. Dora, C. Sasun, Spalling investigation of connecting rod, Eng. Fail. Anal. 19 (2012) 77–86.
[17] A. Afzal, Fatigue Behavior and Life Predictions of Forged Steel and Powder Metal Connecting RodsPhD Thesis University of Toledo, 2004 213–224.
[18] A. Afzal, A. Fatemi, A comparative study of fatigue behavior and life predictions of forged steel and PM connecting rods No. 2004–01-1529, SAE Technical Paper, 2004.
[19] H. Moon, S. Shin, K. Lee, H. Chang, D. Yeom, Development and application of buckling estimation method in engine connecting rod. No. 2007-01-3546, SAE Technical Paper, 2007.
[20] M.K. Lee, H. Lee, T.S. Lee, H. Jang, Buckling sensitivity of a connecting rod to the shank sectional area reduction, Mater. Des. 31 (6) (2010) 2796–2803.
[21] X.L. Xu, Z.W. Yu, Failure analysis of a diesel engine connecting rod, J. Fail. Anal. Prev. 7 (5) (2007) 316–320.
[22] A. Baldini, E. Bertocchi, M. Giacopini, S. Margini, S. Rivasi, R. Rosi, A. Strozzi, On torsional vibrations in conrod assemblies for high performance engines, SISOM 2007 and Homagial Session of the Commission of Acoustics, Bucharest 2008, pp. 426–432.
[23] G.A. Pignone, U.R. Vercelli, Motori ad Alta Potenza Specifica, Giorgio Nada Editore, Vimodrone, 1995.
[24] A. Pioli, A. Strozzi, A. Baldini, M. Giacopini, R. Rosi, Influence of the initial clearance on the peak stress in connecting-rod small ends, Proc. Inst. Mech. Eng. D: J Automob. Eng. 223 (6) (2009) 769–782.
[25] A. Vaccari, Ottimizzazione di Biella in Alluminio: Analisi FEM e Foglio di CalcoloMaster Thesis. University of Modena e Reggio Emilia 2003.
[26] C.F. Taylor, The Internal-Combustion Engine in Theory and Practice: Combustion, Fuels, Materials, Design, 2The MIT Press, Cambridge, 1985.
[27] A. Strozzi, F. De Bona, Hoop stresses in the con-rod small end, Proc. Ints. Mech. Eng. D: J. Automob. Eng 219 (11) (2005) 1331–1345.
[28] A. Londhe, V. Yadav, A. Sen, Finite element analysis of connecting rod and correlation with test. No. 2009-01-0816, SAE Technical Paper, 2009.
[29] M. Ciavarella, P. Decuzzi, The state of stress induced by the plane frictionless cylindrical contact. I. The case of elastic similarity, Int. J. Solids Struct. 38 (26) (2001) 4507–4523.
[30] M. Ciavarella, A. Baldini, J.R. Barber, A. Strozzi, Reduced dependence on loading parameters in almost conforming contacts, Int. J. Mech. Sci. 48 (9) (2006) 917–925.
[31] A. Strozzi, A. Baldini, M. Giacopini, E. Bertocchi, L. Bertocchi, Maximum equivalent stress in a pin-loaded lug in the presence of initial clearance, J. Strain Anal. Eng. Des. (2011) (0309324711423587).
[32] L. Marmorini, A. Baldini, E. Bertocchi, M. Giacopini, R. Rosi, A. Strozzi, On the loosening mechanism of a bush press-fitted in the small end of a connecting rod, Proc. Ints. Mech. Eng. D: J. Automob. Eng 0954407011417498 (2011).
[33] A. Strozzi, P. Vaccari, On the press fit of a crankpin into a circular web in pressed-up crankshafts, J. Strain Anal. Eng. Des. 38 (3) (2003) 189–199.
[34] N. Antoni, Q.S. Nguyen, J.L. Ligier, P. Saffré, J. Pastor, On the cumulative microslip phenomenon, Eur. J. Mech. A. Solids 26 (4) (2007) 626–646.
[35] Y.J. Ahn, E. Bertocchi, J.R. Barber, Shakedown of coupled two-dimensional discrete frictional systems, J. Mech. Phys. Solids 56 (12) (2008) 3433–3440.
[36] C.M. Sonsino, Fatigue design of sintered connecting rods, Met. Powder Rep. 45 (6) (1990) 408–412.
[37] O. Vingsbo, S. Söderberg, On fretting maps, Wear 126 (2) (1988) 131–147.
[38] C. Ruiz, P.H.B. Boddington, K.C. Chen, An investigation of fatigue and fretting in a dovetail joint, Exp. Mech. 24 (3) (1984) 208–217.
[39] D. Merritt, G. Zhu, The prediction of connecting rod fretting and fretting initiated fatigue fracture No. 2004-01-3015, SAE Technical Paper, 2004.
[40] M. Ciavarella, D. Dini, G.P. Demelio, A critical assessment of damage parameters for fretting fatigue, ASTM Spec. Tech. Publ. 1425 (2003) 108–120.
[41] VDI 2230, Part I — Systematic calculation of high duty bolted joints, Joints with one cylindrical bolt, VDI Richtlinien, 31 2003, pp. 145–153.
[42] S.K. Bhaumik, M. Sujata, M.A. Venkataswamy, Fatigue failure of aircraft components, Eng. Fail. Anal. 15 (6) (2008) 675–694.
[43] J.B. Shah, Failure analyses of aircraft accidents – part II, Met. Eng. Q. 14 (4) (1974) 23–25.
[44] R. Rabb, Fatigue failure of a connecting rod, Eng. Fail. Anal. 3 (1) (1996) 13–28.
[45] S. Griza, F. Bertoni, G. Zanon, A. Reguly, T.R. Strohaecker, Fatigue in engine connecting rod bolt due to forming laps, Eng. Fail. Anal. 16 (5) (2008) 1542–1548.
[46] W.D. Webster, R. Coffell, D. Alfaro, A three dimensional finite element analysis of a high speed diesel engine connecting rod No. 831322, SAE Technical Paper, 1983.
[47] K. Kurata, M. Nishikawa, J. Abe, Application of FEM and evaluation method for connecting rod design No. 891770, SAE Technical Paper, 1989.
[48] J.L. Ligier, N. Antoni, Cumulative microslip in conrod big end bearing system, ASME 2006 Internal Combustion Engine Division Spring Technical Conference 2006, pp. 559–567.
[49] M. Pujatti, M. Suhadolc, D. Piculin, Fretting-initiated fatigue in large bore engines connecting rods, Procedia Eng. 74 (2014) 356–359.
[50] M.J. Neale, The Tribology Handbook, II edition Butterworth-Heinemann, 1995.
[51] L. Bertocchi, M. Giacopini, D. Dini, Analysis of the lubrication regimes at the small end and big end of a connecting rod of a high performance motorbike engine, ASME/STLE 2012 Int Joint Trib Conf. 2012, pp. 229–231.
[52] M. Giacopini, L. Bertocchi, A. Baldini, D. Dini, A complementarity formulation for the ehl analysis of a connecting rod big end bearing, World Tribology Congress 2013, Italian Tribology Ass (AIT) 2013, pp. 1–4.
[53] D. Bonneau, D. Guines, J. Frêne, J. Toplosky, EHD analysis, including structural inertia effect and mass-conserving cavitation model, ASME J. Trib. 117 (1995) 540–547.
[54] V. Optasanu, D. Bonneau, Finite element mass-conserving cavitation algorithm in pure squeeze motion: validation/application to a connecting-rod small end bearing, J. Trib. 122 (1) (2000) 162–169.
[55] A. Strozzi, Formulation of three lubrication problems in terms of complementarity, Wear 104 (2) (1985) 103–119.
[56] D. Bonneau, M. Hajjam, Modélisation de la rupture et de la reformation des films lubrifiants dans les contacts élastohydrodynamiques, Rev. Eur. Élém. 10 (6–7) (2001) 679–704.
[57] D.R. Garner, R.D. James, J.F. Warriner, Cavitation erosion damage in engine bearings: theory and practice, J. Eng. Gas Turbines Power 102 (4) (1980) 847–857.
[58] M. Giacopini, M.T. Fowell, D. Dini, A. Strozzi, A mass-conserving complementarity formulation to study lubricant films in the presence of cavitation, J. Tribol. 132 (4) (2010) 041702.
[59] L. Bertocchi, D. Dini, M. Giacopini, M.T. Fowell, A. Baldini, Fluid film lubrication in the presence of cavitation: a mass-conserving two-dimensional formulation for compressible, piezoviscous and non-Newtonian fluids, Tribol. Int. 67 (2013) 61–71.
[60] D. Dini, L.N. Mastrandrea, M. Giacopini, E. Bertocchi, Numerical investigation of the cavitation damage in a high performance engine conrod big end bearing via a mass-conserving complementarity algorithm, Soc. of Tribologists and Lubric Engs Annual Meeting and Exhibition, 2 2014, pp. 586–589.